J Mater Sci (2017) 52:5404–5416

Fabrication of TiO_2/PI composite nanofibrous membrane with enhanced photocatalytic activity and mechanical property via simultaneous electrospinning

Guohong Yang[1], Jiafei Su[1], Yaping Guo[1], He Xu[1,*], and Qinfei Ke[1,*]

[1] *Shanghai Normal University, Shanghai, China*

Received: 17 September 2016
Accepted: 10 January 2017
Published online: 2 February 2017

ABSTRACT

Nanotitanium dioxide (TiO_2)-based materials have attracted an increasing attention in the application of photocatalysis degradation. In this work, a composite TiO_2/PI membrane constructed with anatase TiO_2 and PI nanofibers in an interwoven structure was successfully fabricated by simultaneous electrospinning with a post-annealing process. The results showed that the TiO_2 nanofibers endowed the composite membrane with photocatalytic activity, while the PI nanofibers as the structural reinforcements in the composite membrane could remarkably improve the mechanical property of membrane. Most importantly, the photocatalytic activities and mechanical properties of composite membranes could be further tuned by controlling the TiO_2/PI mass ratio. Our study indicated that the combination of TiO_2 and PI nanofibers via simultaneous electrospinning with a post-annealing process offers a new strategy to construct advanced nano-TiO_2-based materials, which shows a great potential in the application of photocatalytic degradation of toluene.

Introduction

Volatile organic compounds (VOCs) are prevalent components of indoor air pollutants, which significantly impact indoor air quality and thus are harmful for human health. Among VOCs, toluene is a major pollutant [1] and long-term exposure to toluene will result in serious health problems such as headache, upper respiratory tract, eye irritation, leukemia and cancer [2–5]. However, the effective removal of toluene still remains a significant challenge. Photocatalytic oxidation (PCO) has been proved to be a convenient and innovative technology to degrade toluene to CO_2 and H_2O completely in environmental-friendly reaction condition [6–8]. During the process of photocatalytic degradation, nanotitanium dioxide (TiO_2) is the most frequently employed as a photocatalyst, owing to its advantages of excellent chemical stability, good photocatalytic activity,

Address correspondence to E-mail: xuhe@shnu.edu.cn; kqf@shnu.edu.cn

DOI 10.1007/s10853-017-0785-3

nontoxicity and low cost [9, 10]. Currently, many fabrication approaches have been explored to produce nano-TiO_2, such as hydrothermal, sol–gel, co-precipitation and so on. However, the nano-TiO_2 prepared based on these conventional methods is always in the form of particles, which are easily aggregated and largely reduce their photocatalytic activities. Besides, it is difficult to separate and recycle nano-TiO_2 powder during its application, which will result in a second pollution and limit their practical utilization [9, 11].

The emergence of two-dimensional (2D) bulk membranes composed of TiO_2 nanofibers offers an attractive solution to this problem [9]; besides, the TiO_2 nanofibrous membranes possess high specific surface areas and show excellent photocatalytic activities. Among the numerous thin-film fabrication techniques, electrospinning has attracted extensive attention to produce nanosized continuous fibers on account of simple equipment, convenient operation, low cost and wide range of application [12]. Electrospun membranes possess many attractive features, such as controllable fiber diameter, high surface area and variable porosity [9]. Up to now, a lot of efforts have been devoted to fabricating TiO_2 nanofibrous membranes by electrospinning. Generally, precursor TiO_2 fibers are firstly fabricated by electrospinning using a blend of tetrabutyl titanate (TBT) with a carrier polymer, polyvinylpyrrolidone (PVP) in acetic acid and ethanol, and then, PVP is removed after the process of calcination, and finally, TiO_2 nanofibers can be generated [11, 13–20]. However, the TiO_2 nanofibers obtained through this method always result in very poor mechanical properties, and they cannot maintain the structural integrity during the practical application [9]. In fact, it is deviated from the purpose of constructing two-dimensional TiO_2 membranes.

Polyimide (PI), which is a high performance engineering material owing to its excellent mechanical strength, has been widely used as adhesives, dielectrics, filtration membranes and structural reinforcement. More notably, PI is also a kind of high-temperature-resistant material and can be converted from polyamide acid (PAA) fibers through heating process after electrospinning [21–25]. Considering its good mechanical property and resistance to elevated temperature, PI material was chose as a structural reinforcement in the composite membranes in this work. Membranes constructed with PVP/TBT (TiO_2 precursor) and PAA fibers were firstly fabricated by simultaneous electrospinning (as shown in Fig. 1) and then calcined at 400 °C to generate the final composite TiO_2/PI nanofibrous membranes. It is hypothesized that while the TiO_2 nanofibers endow the composite membrane with high photocatalytic activity, the mechanical property of the TiO_2/PI fibrous membranes will be greatly improved compared with the pure TiO_2 nanofibrous membranes, and the mechanical properties and photocatalytic efficiencies of the composite membranes could be further tuned by controlling the mass ratios of TiO_2/PI.

In this work, four kinds of composite membranes with different TiO_2/PI mass ratios were fabricated through simultaneous electrospinning with a post-annealing process, and their morphologies and structures were subsequently evaluated. Finally, the mechanical properties and photocatalytic properties of composite membranes with different TiO_2/PI mass ratios were systematically studied, and the possible mechanism was proposed.

Experimental

Materials and method

Polyvinylpyrrolidone (PVP, Aladdin, $M_W = 58000$), 4,4′-oxydianiline (ODA, Aladdin, 98%), pyromellitic dianhydride (PMDA, Aladdin, 96%) and tetrabutyl titanate (TBT, Aladdin, ≥99.0%) were all purchased from Sinopharm Chemical Reagent Co., Ltd. (Shanghai, China). Acetic acid (Enox, AR), *N*, *N*-dimethylformamide (DMF), ethanol and acetone were of analytical grade and supplied by Rich Joint Chemical Reagent Co., Ltd. (Shanghai, China). All the reagents were used as received without any further purification.

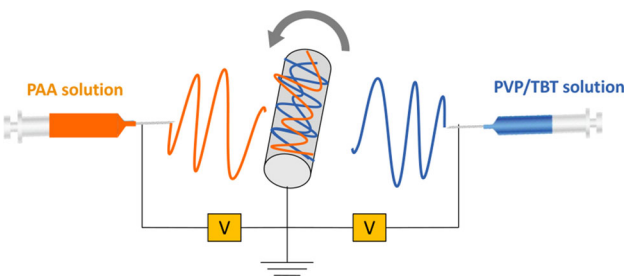

Figure 1 Schematic illustration of the simultaneous electrospinning process of PVP/TBT/PAA composite membranes.

Fabrication of TiO_2/PI composite membranes

Preparation of PVP/TBT solution

6.5 g PVP was dissolved in 10 mL ethanol under vigorous stirring for 5 h to obtain a homogeneous solution. TiO_2 precursor solution was prepared through dipping 3.3 mL TBT into 6.6 mL acetic acid under vigorous stirring for 2 h. After that, the TiO_2 precursor solution was dipped into PVP solution and stirred for another 10 h to obtain PVP/TBT solution. All experiments were carried out at room temperature.

Preparation of PAA solution

First, DMF solvent was added into ODA under mechanical stirring in a three-necked flask, and then, PMDA was added into the above solution gradually to obtain PAA solution. The mole ratio of ODA and PMDA was 1:1.02, and the concentration of the solution was 20 wt%.

Preparation of TiO_2/PI composite membranes

As shown in Fig. 1, the simultaneous electrospinning process was carried out using a TEADFS-103 electrospinning apparatus composed of one rotating drum collector, two positive DC voltage supplies and two syringe pumps (Beijing Technova Technology Co., Ltd). The two syringe pumps were placed on opposite sides of the drum collector. During the simultaneous electrospinning process, the PVP/TBT solution and PAA solution were loaded into the two syringes, respectively. For the preparation of PAA electrospun nanofibers, the solution was fed at a constant rate by a syringe pump through a stainless steel needle with inner diameter of 0.99 mm. The voltage applied to the needle of the syringe was 15 kV. The distance between the tip of the needle and the collector was 10 cm. Meanwhile, the PVP/TBT electrospun nanofibers were fabricated under the following condition: the inner diameter of needle was 0.99 mm, the applied voltage was 10 kV, and the tip-to-collector distance was 12 cm. The rate of roller was 800 r/min, and the collecting time for all samples was fixed for 100 min.

To obtain the final TiO_2/PI composite membranes, the PVP/TBT/PAA composite membranes were further calcined in the furnace. The programmed temperature process was set as follows: the membranes were heated up to 80 °C for 1 h, 160 °C for 30 min, 200 °C for 30 min, 250 °C for 30 min, 300 °C for 2 h, 350 °C for 2 h and then 400 °C for 3 h. During this process, the heating rate was set as 2 °C/min.

The mass ratios of the TiO_2/PI composite membranes were controlled by altering the feeding rate ratios of PVP/TBT and PAA solution during the simultaneous electrospinning process. For instance, a TiO_2/PI composite membrane named as T1P1 was fabricated by fixing the feeding rate of PVP/TBT solution at 0.02 mL/min and PAA solution at 0.02 mL/min, respectively. In this way, four kinds of TiO_2/PI composite membranes with different content of TiO_2 were obtained by controlling the feeding rate ratios of 0:1, 1:2, 1:1, 2:1 and 2:0 ((PVP/TBT)/PAA), and the corresponding samples were named as PI, T1P2, P1T1, T2P1 and TiO_2, respectively. The accurate content of TiO_2 in each sample was calculated using the formula as follows:

$$\omega_T = \frac{w_T}{W} \tag{1}$$

where ω_T is the content of TiO_2, w_T is the mass of TiO_2 transformed from the PVP/TBT spinning solution, and W is the total mass of the sample. The contents of TiO_2 in PI, T1P2, T1P1, T2P1 and TiO_2 samples are shown in Table S1.

Characterization

Morphology observation of TiO_2/PI electrospun membranes

The morphologies and microstructures of the composite electrospun membranes were characterized by field emission scanning electron microscopy (FE-SEM, HitachiS-4800, CanScan).

The composition, phases and functional groups of TiO_2/PI electrospun membranes

The chemical composition of the prepared membranes was characterized by energy-dispersive spectrum (EDS). The X-ray powder diffraction (XRD, D/max-IIB, Japan) was used to examine the phases of samples by using CuKα radiation ($\lambda = 1.541874$ Å) within the scanning range of $2\theta = 10°$–$80°$ at a scanning rate of $6°\ \text{min}^{-1}$ and a step size of 0.02°. The functional groups of samples were further

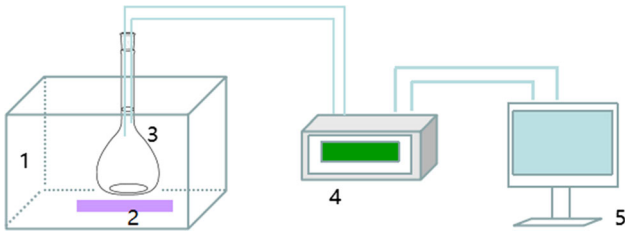

Figure 2 Schematic illustration of the process of photocatalytic test (*1* dark box; *2* ultraviolet lamp; *3* volumetric flask; *4* photoacoustic IR multigas monitor; *5* computer.).

determined by Fourier transform infrared spectra (FTIR, Nicolet 5DX).

The mechanical properties of TiO_2/PI electrospun membranes

The mechanical properties of the prepared membranes were measured by a mechanical testing machine (WDW-0.5C, Shanghai HUALONG Testing Instrument Co., Ltd., China). Before the test, the samples were cut into strips with area of 50×10 mm^2. The thickness value of each sample was measured by digital fabric thickness tester (YG141D, Chang Yi Fang Yi Co., Ltd., China). The samples were clamped by two tensile fixtures, and the distance between two tensile fixtures was set as about 30 mm. The moving speed of the tensile fixtures was 10 mm min^{-1}. At least one group of five samples was used for each test to obtain an average value. All tests were carried out at room temperature.

The Brunauer–Emmett–Teller (BET) surface area measurements of electrospun membranes

The BET surface areas of samples were determined using N_2 adsorption–desorption isotherms with a surface area analyzer (ASAP 2020, Micromeritics Co., USA), and the adsorption data under the relative pressure P/P_o with the range of 0.05–0.9 were recorded.

Photocatalytic test

The photocatalytic activities of the prepared membranes were evaluated by the degradation of toluene under the irradiation of a 40-W ultraviolet (UV) lamp in a laboratory-made reaction device at room temperature. The data were further analyzed by an online photoacoustic IR multigas monitor (INNOVA air Tech Instruments Model 1412i). The schematic illustration of the photocatalytic test is shown in Fig. 2.

In a typical process, the prepared membrane (40 cm^2) was put into the volumetric flask (1 L), and then, the flask was sealed with a rubber plug; finally, 1 μL concentrated toluene was injected into the flask device by a microsyringe. The initial concentration of toluene was about 400 ± 50 mg/m^3. The mixture was kept in the dark to gain a good dispersion and established an adsorption–desorption equilibrium between the samples and toluene. After that, the UV lamp was lighted up when the concentration of toluene remained unchanged for 2 h and then the test was kept for 2 days. During this test, both the concentrations of toluene and carbon dioxide (the product of degradation) were recorded to evaluate the photocatalytic performance of the samples. The room temperature was kept at 20 ± 5 °C during the photodegradation process.

The conversion rate of toluene for different samples was calculated by the increment of CO_2 using the following formula:

$$\text{Toluene coversion } (\%) = \frac{\Delta CO_2}{(CO_2)_T} \times 100\% \quad (2)$$

where ΔCO_2 is the increased CO_2 concentration during the photocatalysis test and $(CO_2)_T$ is the theoretical amount of CO_2 produced when 1 μL toluene is degraded completely.

Statistical analysis

The results were expressed as the arithmetic mean ± SD. Three independent experiments were carried out, and at least five samples per test were taken for statistical analysis. Statistical significance between two groups was calculated using two-tailed analysis of variance (ANOVA) and performed with a Student's *t* test program. Differences were considered significantly when $p < 0.05$ (*), $p < 0.01$ (**) or $p < 0.001$ (***). In addition, a one-way ANOVA with Tukey's post hoc test was used for statistical analysis of multiple comparisons. Significant difference was considered when $p < 0.05$ (*), $p < 0.01$ (**) or $p < 0.001$ (***).

Results and discussion

The fabrication of TiO_2/PI composite electrospun membranes with different mass ratios

The morphologies of TiO_2/PI electrospun membranes with different mass ratios are shown in Fig. 3. Figure 3a_1–e_1 shows the SEM images of samples before being calcined, revealing that the as-spun nanofibers were continuous and the nanofibers in those membranes were randomly deposited in interwoven network structures. As observed, the pure PAA precursor nanofibers were relatively straight and the average diameter of nanofibers was about 850–910 nm (Fig. 3a_1). Similar to the PAA electrospun membrane, the nanofibers in PVP/TBT electrospun membrane also exhibited uniform nanostructures with an average diameter of 830–950 nm (Fig. 3e_1). However, different from those pure PAA or PVP/TBT nanofibrous membranes with uniform fiber diameter, the composite PVP/TBT/PAA electrospun membranes showed the diameter of nanofibers in an uneven distribution (Fig. 3b_1–d_1).

Figure 3a_2 shows the SEM images of PI electrospun membranes after being calcined. It was clear to see that there was no much change in the morphologies of PI nanofibers during the calcination process, and the PI nanofibers were still continuous and straight with the fiber diameter of 290–700 nm, while the TiO_2 nanofibers had been cracked into short rod-like structures with the length in the range of 500–5000 nm and the diameter about 140–305 nm (Fig. 3e_2).

Figure 3b_2–d_2 shows that the morphologies of the TiO_2/PI composite membranes were remarkably changed after being calcined. In contrast to those pure TiO_2 or PI nanofibrous membranes, there were cracked short rod-like TiO_2 fibers randomly interweaved with the continuous PI fibers, and the cracked fibers in the composite membranes were significantly increased with the increase in TiO_2/PI mass ratio. Corresponding to the SEM images, the photographs of samples with different TiO_2/PI mass ratios are shown in Fig. S1; it also can be seen that the pure TiO_2 samples exhibited powder-like appearance, while the others were 2-D bulk membranes.

In addition, it was worth mentioning that the PI nanofibers in the composite membranes had changed into curved shapes. This phenomenon can be explained as follows. After the simultaneous electrospinning process, the obtained precursor composite membranes were constructed with PVP/TBT and PAA nanofibers in randomly crossed structures. However, during the calcination process, the TiO_2 nanofibers showed dramatical dimensional shrinkage behavior mainly due to the removal of PVP in the precursor nanofibers, which would pull the bonding PI nanofibers and resulted in the curved shapes of PI nanofibers. Moreover, the bonding points between TiO_2 and PI nanofibers were increased with the increasing TiO_2/PI mass ratio, which would result in more curved structures of PI nanofibers.

Energy-dispersive spectrum (EDS) analysis in Fig. 4 showed the element distribution of electrospun membranes. As observed, only C and O elements were detected in the pure PI membrane, while there were obvious Ti signals shown in the composite

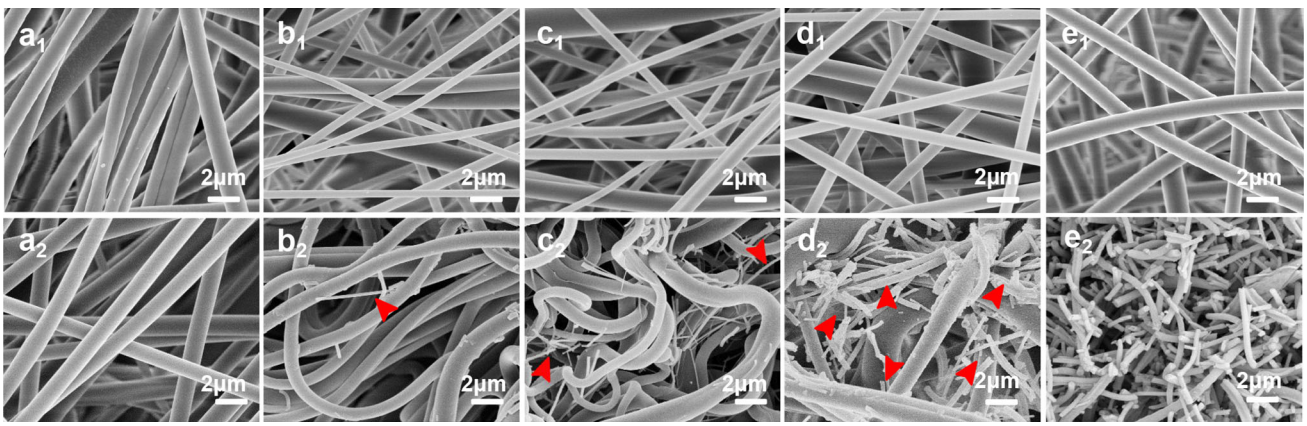

Figure 3 FE-SEM images of TiO_2/PI electrospun membranes with different mass ratios [(a_1–a_2) PI, (b_1–b_2) T1P2, (c_1–c_2) T1P1, (d_1–d_2) T2P1 and (e_1–e_2) TiO_2 before (a_1–e_1) and after being calcined (a_2–e_2)]. *Red arrows* pointed the TiO_2 nanofibers in the composite membranes.

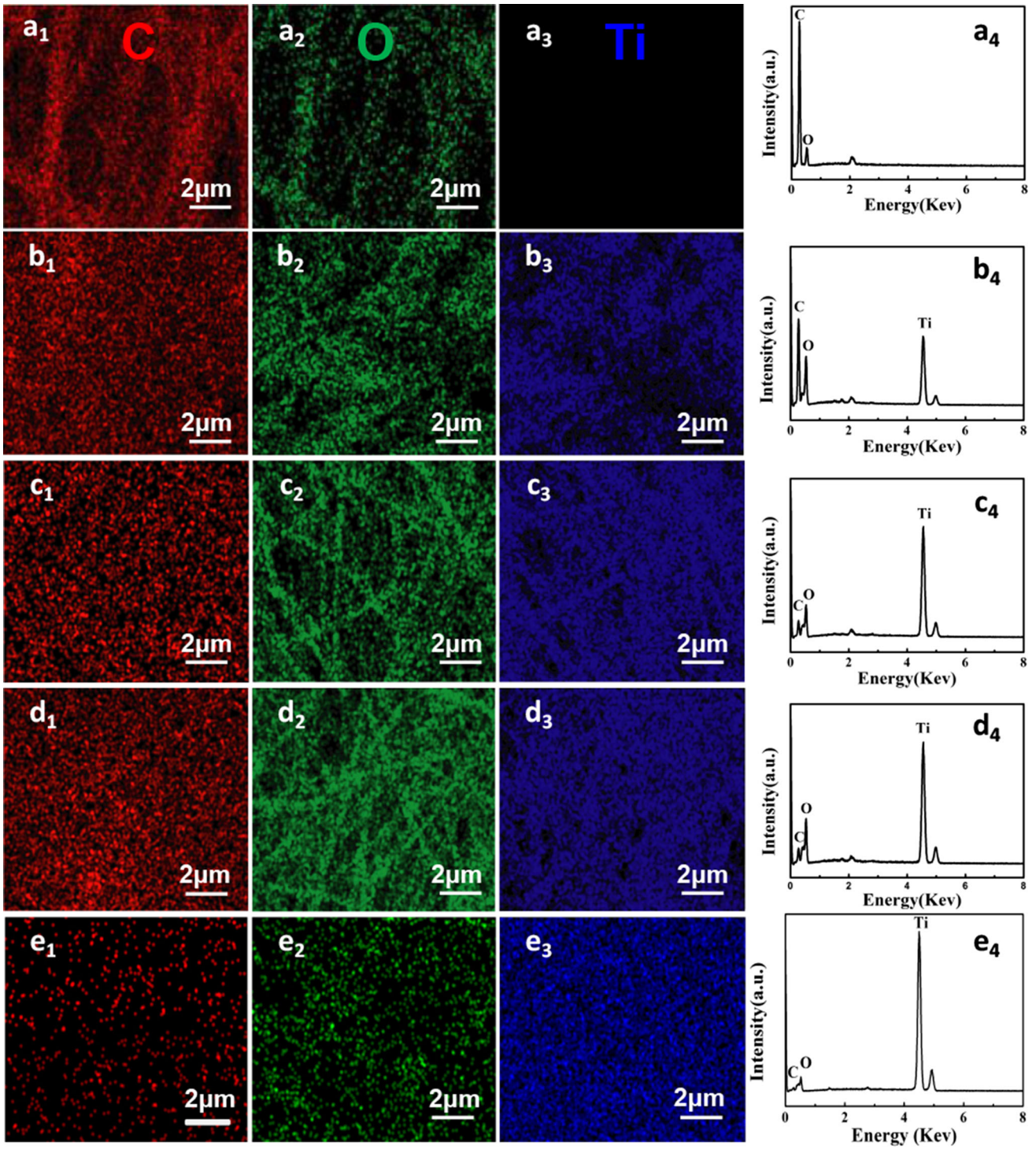

Figure 4 Elemental mapping analysis showed C element (a_1–d_1), O element (a_2–d_2) and Ti element (a_3–d_3) distributed in the electrospun membranes with different TiO_2/PI mass ratios: (a_1–a_3) PI; (b_1–b_3) T1P2; (c_1–c_3) T1P1; (d_1–d_3) T2P1; (e_1–e_3) TiO_2 fibers. The intensity of elements contents in the corresponding samples are shown in graphs a_4, b_4, c_4, d_4, respectively.

membranes. Moreover, it was clear to see that the Ti signal became much stronger with the increase in TiO_2/PI mass ratio, which meant that the contents of Ti were increased in the composite membranes. The corresponding elements contents are shown in Fig. 4a$_4$–d$_4$, and the results indicated that the

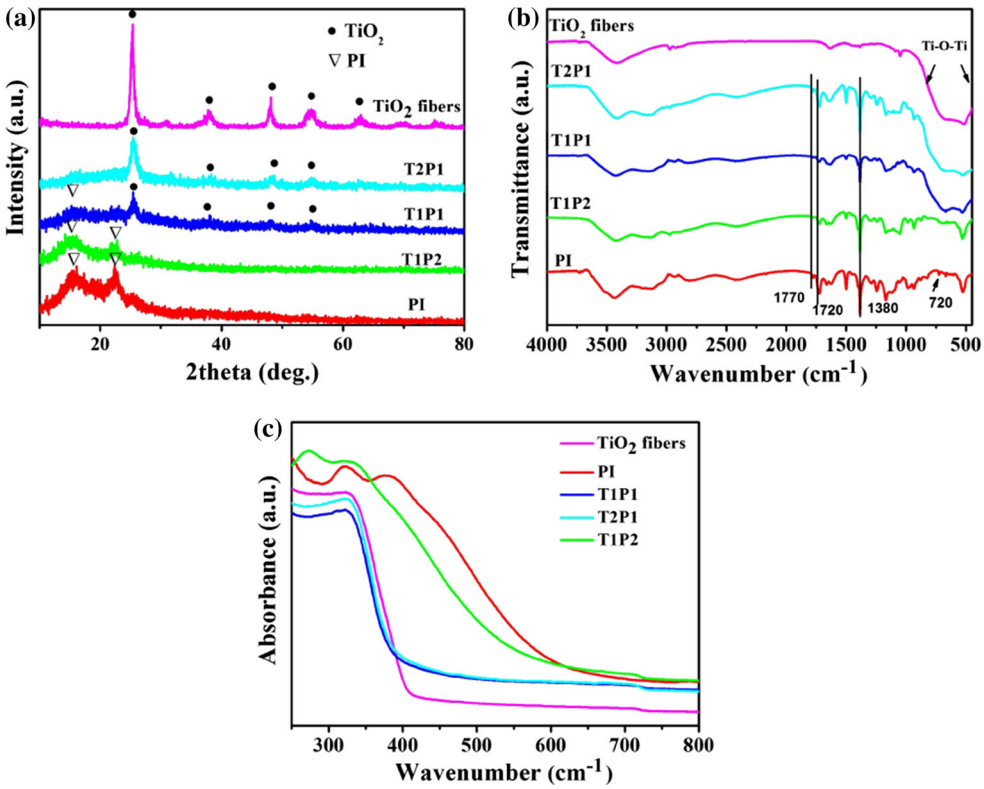

Figure 5 X-ray diffraction patterns (**a**), FTIR spectra (**b**) and UV–Vis absorbance spectra (**c**) of the electrospun scaffolds with different TiO_2/PI mass ratios.

contents of Ti element in the composite membranes ranged from 4.41 to 40.68% with the increasing TiO_2/PI mass ratio.

X-ray diffraction (XRD) analysis of the electrospun membranes is shown in Fig. 5a. Compared with the only amorphous phase existed in the pure PI membranes, the strong peaks at 25.6°, 38.2°, 48.2°, 54.1° and 63.1° assigned to the reflections of (101), (004), (200), (211) and (204) crystal planes of the anatase phase of TiO_2 (JCPDS No. 21-1272) were detected in the T1P1, T2P1 and pure TiO_2 membranes, revealing that the PVP/TBT nanofibers in the composite membrane had been transformed to anatase TiO_2 nanofibers completely. However, there were no diffraction peaks of anatase phase of TiO_2 observed in the case of T1P2, mainly due to the low amount of TiO_2 nanofibers in the membranes, and with the increase in TiO_2/PI mass ratio, the characteristic phases of TiO_2 in the composite membranes became more and more obvious.

The chemical structures of the electrospun membranes were further investigated by Fourier transform infrared spectroscopy (FTIR). As shown in Fig. 5b, there were C=O (1770, 1720, 720 cm^{-1}) and C–N (1380 cm^{-1}) bonds detected in the pure PI membranes [26]. In contrast, new peaks appeared at 550–850 cm^{-1} in the composite TiO_2/PI and pure TiO_2 membranes, which was assigned to Ti–O–Ti stretching bond, and its absorbance intensity was increased with the increase in TiO_2/PI mass ratio. These results confirmed the fact that the TiO_2/PI composite electrospun membranes were successfully fabricated after the simultaneous electrospinning and calcination process.

The optical absorption properties of the samples were measured by UV–Vis absorbance spectra. As shown in Fig. 5c, remarkable absorption appeared at the UV region from 250 to 400 nm for both the T1P1 and T2P1 membranes, which revealed that the incorporation of PI nanofibers in the composite membranes had not changed the ultraviolet absorption behavior of TiO_2 fibers [27]. However, the absorption edge of pure PI membrane extended to the visible wavelength of 600 nm, and the additional visible light absorption may be related to the color of as-prepared PI membrane changing from white to yellow during the calcination process. Otherwise, this absorption behavior could also be found in the T1P2 membrane, which was composed of much more PI nanofibers compared with the other two composite samples.

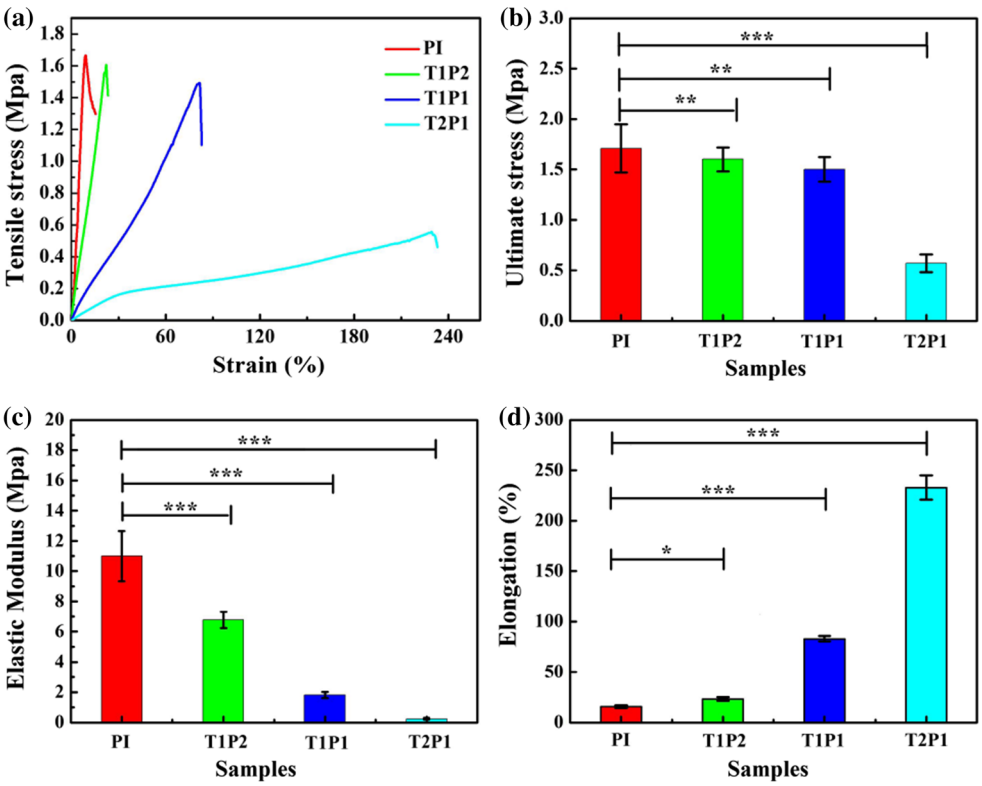

Figure 6 Stress–strain curves (**a**), tensile strengths (**b**), elastic moduli (**c**) and elongation (**d**) of the composite electrospun scaffolds with different TiO_2/PI mass ratios (*, ** and *** represent $p < 0.05$, $p < 0.01$ and $p < 0.001$, respectively).

Mechanical properties

To further investigate the effect of TiO_2/PI mass ratio on the mechanical properties of composite membranes, the tensile strengths, elastic modulus and break elongation of the membranes were evaluated. As shown in Fig. 6a, all the membranes exhibited linear elastic behaviors at relatively lower stress zone, while they exhibited nonlinear elastic behaviors when the stress reached to the yield point and finally the membrane broke [28, 29]. The pure PI membrane showed the maximum stress and elastic modulus among all the samples with the ultimate stress and elastic modulus values of 1.71 and 10.99 Mpa, respectively, while the T2P1 composite membranes with the most TiO_2 nanofibers showed the minimum values of 0.57 and 0.24 Mpa, respectively, and the ultimate stress and elastic modulus of the composite membranes were significantly decreased with the increase in TiO_2 mass ratio (Fig. 6b, c). Due to the nature of the chemical structure consisting rigid heterocyclic imide rings and aromatic rings on the backbone, PI exhibits excellent mechanical property as well as high thermal stability [30, 31]. In this work, PI polymer was chosen as a mechanical reinforcement in the composite membrane. As PI and TiO_2 nanofibers were randomly deposited to construct an interwoven network structure in the composite membrane, the crossed PI nanofibers could cover up the fragile characteristics of TiO_2 fibers and greatly improve the strengths of the composite membranes. In addition, the mechanical strengths of the composite membranes could be further enhanced by the increase in PI nanofibers [32]. However, it could be also found that the break elongation of the membranes showed contrary tendency, the break elongation of the composite membranes were significantly increased from 15.55 to 233.05% with the increase in TiO_2/PI mass ratio, and the composite membranes with the most TiO_2 nanofibers possess the highest elongation. As is aforementioned, the PI nanofibers in the composite membranes exhibited curved shapes, it is speculated that the elongation of composite membranes may be attributed to the special structure of PI nanofibers [32, 33]. When there is an external load, the curved PI nanofibers tend to be straightened and the membranes would exhibit constantly elongated behaviors. In this case, with the increase in TiO_2 nanofiber, the elongations of composite membranes show gradually increased behaviors owing to the more curved structures of PI nanofibers.

These results indicate that both the material itself and the geometric arrangement of fibers could largely affect the mechanical property of nanofibrous membrane. By altering the TiO_2/PI mass ratio, the mechanical properties of composite membranes could be well controlled and the T1P1 shows the most balanced mechanical properties with both high tensile strengths and break elongation.

Photocatalytic activity

Photocatalytic activities of the samples with different TiO_2/PI mass ratios were investigated by the degradation of toluene under ultraviolet irradiation. As shown in Fig. 7a, the concentration of toluene in each test was significantly decreased in a short time after injecting toluene solution into the reactor, especially for that of composite membranes, revealing that a strong adsorption of the membrane to toluene gas was occurred during the process. After a period of time, it reached an adsorption equilibrium between the membrane and toluene. However, the ultimate concentration of toluene was different for each test of sample, and the toluene concentration was lower when more TiO_2 fibers were incorporated in the composite membranes. Compared with the pure PI nanofibrous membranes, all the TiO_2/PI composite membranes showed strong adsorption capacity to toluene (Fig. 7b). The BET measurement in Fig. 8 showed that the surface areas of the composite membranes were higher when more TiO_2 fibers were incorporated, and the surface area of the pure TiO_2 nanofibers was the highest among all the samples with the value of 49.01 $m^2\ g^{-1}$. It is speculated that the increase in surface area is closely related to the smaller diameter of TiO_2 nanofibers. In this case, the

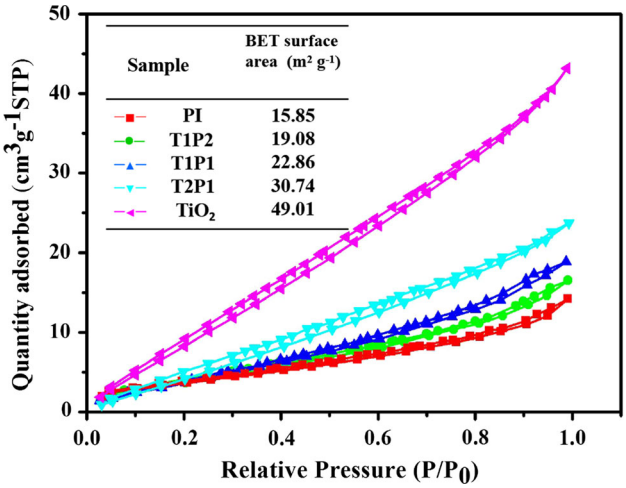

Figure 8 N_2 adsorption–desorption isotherms and BET surface areas of samples with different TiO_2/PI mass ratios.

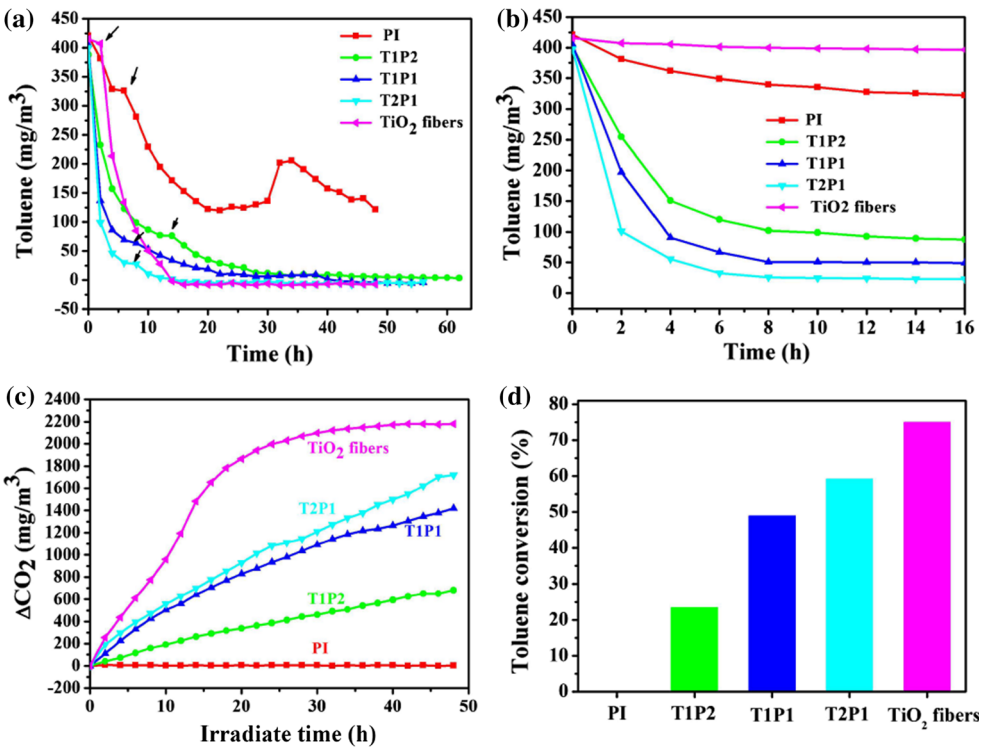

Figure 7 **a** Changes in the concentration of toluene throughout the test (*the arrows* showed the time point of turning UV lamp on.); **b** changes in the concentration of toluene without UV radiation; **c** changes in the CO_2 concentrations as a function of reaction time with UV radiation; **d** the efficiency of toluene conversion for the samples with different TiO_2/PI mass ratios.

incorporation of TiO_2 fibers could endow the composite membranes with larger specific surface area and provide more active sites [4]. So it could come to a conclusion that a large number of adsorption sites on the composite membranes are beneficial to rapid diffusion of toluene, thereby increasing the adsorption capacity. It is also mentioned that the pure TiO_2 fibers exhibited different behavior compared with other samples and there was no remarkable adsorption to toluene before turning on the ultraviolet lamp; it is mainly due to the powder-like appearance of TiO_2 samples (Fig. S1), in which the short TiO_2 nanofiber stacked together and largely reduced the contact area of the sample between toluene.

After turning on the ultraviolet lamp, as the arrow showed the time point in Fig. 7a, the concentration of toluene dramatically declined in the presence of as-prepared samples with the extending UV irradiation time, and it could be noticed that all the samples that contain the TiO_2 fibers could eliminate toluene completely and the concentration of toluene reached 0 mg m^{-3} in the end. In contrast to those samples, the pure PI membrane exhibited a quite different behavior; the concentration of toluene decreased at a slower speed compared with other samples and reached to the adsorption–desorption equilibrium firstly but increased after turning on the ultraviolet lamp for a period of time until the adsorption–desorption equilibrium was achieved again. It is speculated that the exceptional increase in toluene may be due to the rising temperature of the reactor after being irradiated by UV lamp, resulting in the desorption of toluene on the surface of PI fibers. This speculation was further evidenced by the formation rate of CO_2 in the test of PI membrane. As shown in Fig. 7c, it was clear to see that there was no additional CO_2 produced during the PI test, which revealed that the toluene was physically captured by PI nanofibers and the adsorption behavior was easily influenced by the temperature of reactor during the process of test. However, it was also noted that the CO_2 concentrations were remarkably increased with irradiation time in the tests of other samples that contained TiO_2 fibers, which indicated that the toluene could be degraded to CO_2 in the presence of TiO_2 fibers, and the photocatalytic activities of the membranes were significantly improved with the increased amount of TiO_2 nanofibers. After being irradiated by ultraviolet

Table 1 Toluene conversion of different samples ($(CO_2)_T = 2904$ (mg m^{-3}))

	PI	T1P2	T1P1	T2P1	TiO_2 fibers
ΔCO_2 (mg m^{-3})	0	681.16	1419.23	1718.99	2176.85
Toluene conversion (%)	0	23.46	48.87	59.19	74.96

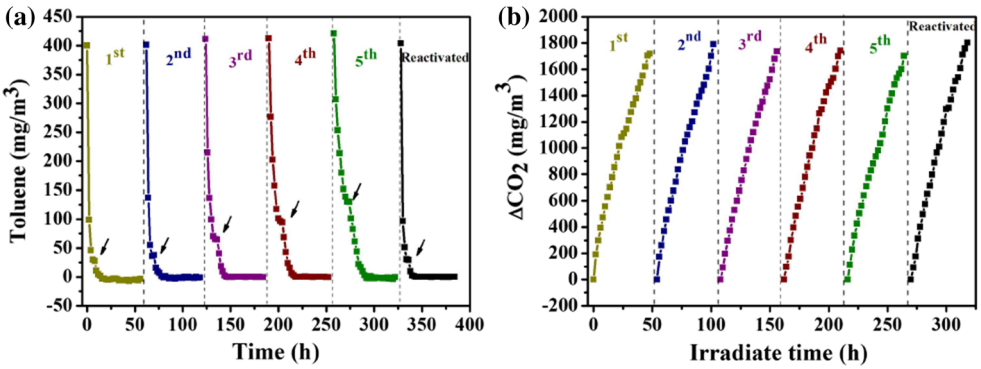

Figure 9 Changes in toluene (**a**) and CO_2 (**b**) concentration with reaction time for T2P1 in the recycle tests (*the arrows* showed the time point of turning UV lamp on).

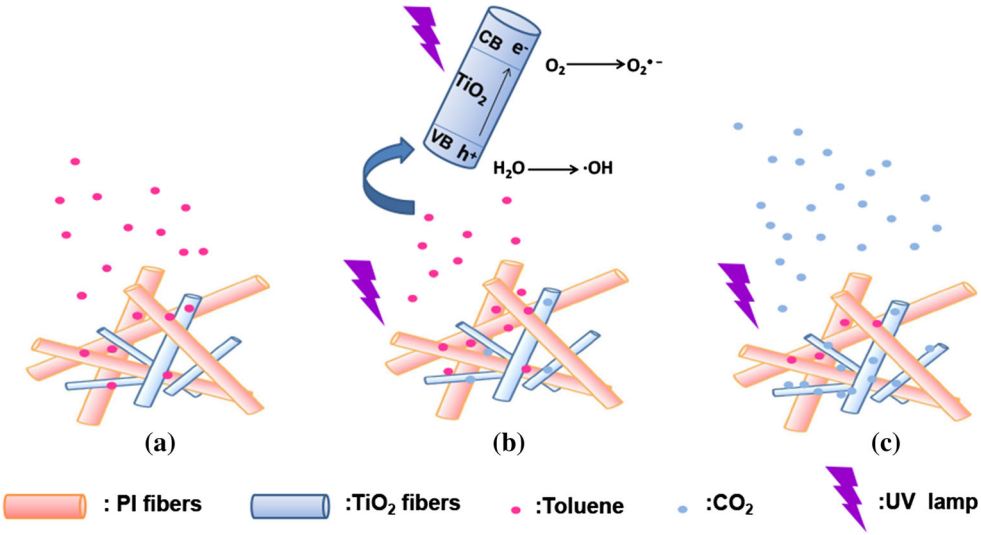

Figure 10 Proposed mechanism of the effect of TiO_2/PI composite electrospun membrane in the toluene photocatalytic degradation process.

lamp for 48 h, the generation of CO_2 was 681.16, 1419.23, 1718.99 and 2176.85 mg m^{-3} for T1P2, T1P1, T2P1 membranes and TiO_2 fibers, respectively. The toluene conversion rates of different samples were further evaluated, and the results are shown in Fig. 7d and Table 1. TiO_2 fibers exhibited the highest toluene conversion efficiency (74.96%), while the toluene conversion rate of toluene in the test of PI membrane was 0%, and the toluene conversion rate was increased with the increase in TiO_2/PI mass ratio. These results indicated that the content of TiO_2 had a major impact on the photocatalytic ability of composite membranes.

The stability of catalyst is also a critical factor in practical application [37]. The recycle experiments ($n = 5$) had been performed by using T2P1 sample as model, and the result is shown in Fig. 9. The changes in toluene concentrations in the five recycles showed remarkable difference before turning on the UV lamp. However, the sample could be reactivated after being dried at 80 °C for 12 h in vacuum, and the changes in toluene concentrations are consistent with that in the first recycle. Besides, after turning on the UV lamp, there are no remarkable changes in toluene concentrations and the production of CO_2 is consistent with that in the first recycle as well, suggesting that the as-prepared sample can keep a stable and efficient catalytic performance [38].

The proposed mechanism of the photocatalytic degradation of TiO_2/PI composite membranes is shown in Fig. 10. When the toluene molecule is in contact with the surface of the TiO_2/PI composite membrane, part of the molecules is physically captured by PI nanofibers, while the rest is directly adsorbed by the TiO_2 nanofibers to participate in the photocatalytic reaction under ultraviolet irradiation. Since adsorption process is the first step involved in the UV-PCO method (Fig. 10a), the larger specific surface areas of TiO_2/PI composite membranes with more active sites to rapidly absorb toluene molecule are helpful to increase their photocatalytic activities. Beyond that, the increased short rod-like TiO_2 nanofibers in the composite membranes could generate more positive hole-negative electron pairs to produce ·OH radicals and superoxide radical anion ($O_2^{\cdot-}$) [34–36] (Fig. 10b) and finally degrade toluene to CO_2 (Fig. 10c) with higher efficiency.

These results indicate that under the same condition of UV irradiation, the photocatalytic activities of samples could be enhanced by the addition of TiO_2 nanofibers and further be controlled by the TiO_2/PI mass ratios in the composite membranes. As it turns out, both of the T2P1 and T1P1 composite membranes exhibited high removal efficiencies of toluene. Therefore, considering a balance between the mechanical property and photocatalytic activity, the T1P1 composite membrane might be the most suitable candidate for the potential application in toluene photocatalytic degradation.

Conclusions

In this work, the TiO_2/PI composite membranes with different TiO_2/PI mass ratios were successfully fabricated by simultaneous electrospinning with a post-

annealing process. The results showed that the TiO_2 and PI nanofibers were randomly deposited in the membranes with interwoven structures, and the mechanical properties of the membranes could be improved with the cooperation of PI nanofibers as structural reinforcements, while the TiO_2 nanofibers endowed the composite membranes with photocatalytic activities. Most importantly, the photocatalytic activities and mechanical properties of composite membranes could be further tuned by controlling the TiO_2/PI mass ratio, and the T1P1 sample showed the most balanced property with high photocatalytic activity and mechanical strength for the potential application in toluene photocatalytic degradation. The results suggest that our work offers a new strategy to construct advanced nano-TiO_2-based materials, which could overcome the relatively low recuperability and reutilization limitation of the current TiO_2 materials in the commercial applications.

Acknowledgements

Funding for this study was provided by the Project of Local Capacity Construction of Shanghai Municipal Science and Technology Commission (No. 14520502800), National Natural Science Foundation of China (No. 81501597), Yangfan Program of Shanghai Science and Technology Committee (NO. 15YF1408900) and China Postdoctoral Science Foundation (2015M580341).

Electronic supplementary material: The online version of this article (doi:10.1007/s10853-017-0785-3) contains supplementary material, which is available to authorized users.

References

[1] Kim J, Zhang P, Li J, Wang J, Fu P (2014) Photocatalytic degradation of gaseous toluene and ozone under UV254 + 185 nm irradiation using a Pd-deposited TiO_2 film. Chem Eng J 252:337–345

[2] Nie L, Yu J, Li X, Cheng B, Liu G, Jaroniec M (2013) Enhanced performance of NaOH-modified Pt/TiO_2 toward room temperature selective oxidation of formaldehyde. Environ Sci Technol 47:2777–2783

[3] James RN, Collins J, Tyl Rochelle W, Krivanek Neil, Esmen Nurtan A, Hall Thomas A (2001) A review of adverse pregnancy outcomes and formaldehyde. Regul Toxicol Pharmacol 34:17–34

[4] Yan Z, Xu Z, Yu J, Jaroniec M (2015) Highly active mesoporous ferrihydrite supported pt catalyst for formaldehyde removal at room temperature. Environ Sci Technol 49:6637–6644

[5] Daisey WJAJM, Apte MG (2003) Indoor air quality, ventilation and health symptoms in schools: an analysis of existing information. Indoor Air 13:53–64

[6] Lannoy A, Kania N, Bleta R, Fourmentin S, Machut-Binkowski C, Monflier E, Ponchel A (2016) Photocatalysis of volatile organic compounds in water: towards a deeper understanding of the role of cyclodextrins in the photodegradation of toluene over titanium dioxide. J Colloid Interface Sci 461:317–325

[7] Mo J, Zhang Y, Xu Q, Lamson JJ, Zhao R (2009) Photocatalytic purification of volatile organic compounds in indoor air: a literature review. Atmos Environ 43:2229–2246

[8] Zuo GM, Cheng ZX, Chen H, Li GW, Miao T (2006) Study on photocatalytic degradation of several volatile organic compounds. J Hazard Mater 128:158–163

[9] Renzhong Zhang XW, Song Jun, Si Yang, Zhuang Xingmin, Jianyong Yu, Ding Bin (2015) In situ synthesis of flexible hierarchical TiO_2 nanofibrous membranes with enhanced photocatalytic activity. J Mater Chem A 3:22136–22144

[10] Al Momani F (2007) Treatment of air containing volatile organic carbon: elimination and post treatment. Environ Eng Sci 24:1038–1047

[11] Yang Y, Wang H, Li X, Wang C (2009) Electrospun mesoporous W^{6+}-doped TiO_2 thin films for efficient visible-light photocatalysis. Mater Lett 63:331–333

[12] Baji A, Mai Y-W, Wong S-C, Abtahi M, Chen P (2010) Electrospinning of polymer nanofibers: effects on oriented morphology, structures and tensile properties. Compos Sci Technol 70:703–718

[13] Wang X, Choi J, Mitchell DRG, Truong YB, Kyratzis IL, Caruso RA (2013) Enhanced photocatalytic activity: macroporous electrospun mats of mesoporous Au/TiO_2 nanofibers. ChemCatChem 5:2646–2654

[14] Tang C, Hu M, Fang M, Liu Y, Wu X, Liu W, Wang M, Huang Z (2015) Photocatalytic property of TiO_2-vermiculite composite nanofibers via electrospinning. Nanoscale Res Lett 10:276–281

[15] Shen J, Wu Y-N, Fu L, Zhang B, Li F (2013) Preparation of doped TiO_2 nanofiber membranes through electrospinning and their application for photocatalytic degradation of malachite green. J Mater Sci 49:2303–2314. doi:10.1007/s10853-013-7928-y

[16] Mondal K, Bhattacharyya S, Sharma A (2014) Photocatalytic degradation of naphthalene by electrospun

mesoporous carbon-doped anatase TiO_2 nanofiber mats. Ind Eng Chem Res 53:18900–18909

[17] Madhugiri S, Sun B, Smirniotis PG, Ferraris JP, Balkus KJ (2004) Electrospun mesoporous titanium dioxide fibers. Microporous Mesoporous Mater 69:77–83

[18] Du P, Song L, Xiong J, Cao H (2013) Photocatalytic degradation of Rhodamine B using electrospun TiO_2 and ZnO nanofibers: a comparative study. J Mater Sci 48:8386–8392. doi:10.1007/s10853-013-7649-2

[19] Alves AK, Berutti FA, Bergmann CP (2013) Visible and UV photocatalytic characterization of Sn–TiO_2 electrospun fibers. Catal Today 208:7–10

[20] Zhang X, Xu S, Han G (2009) Fabrication and photocatalytic activity of TiO_2 nanofiber membrane. Mater Lett 63:1761–1763

[21] Jiang S, Duan G, Chen L, Hu X, Hou H (2015) Mechanical performance of aligned electrospun polyimide nanofiber belt at high temperature. Mater Lett 140:12–15

[22] Li XJ, Wei Q, Wang X (2014) Preparation of magnetic polyimide/maghemite nanocomposite fibers by electrospinning. High Perform Polym 26:810–816

[23] Liu J, Huang J, Wujcik EK, Qiu B, Rutman D, Zhang X, Salazard E, Wei S, Guo Z (2015) Hydrophobic electrospun polyimide nanofibers for self-cleaning materials. Macromol Mater Eng 300:358–368

[24] Wang Q, Song W-L, Wang L, Song Y, Shi Q, Fan L-Z (2014) Electrospun polyimide-based fiber membranes as polymer electrolytes for lithium-ion batteries. Electrochim Acta 132:538–544

[25] Zha J-W, Sun F, Wang S-J, Wang D, Lin X, Chen G, Dang Z-M (2014) Improved mechanical and electrical properties in electrospun polyimide/multiwalled carbon nanotubes nanofibrous composites. J Appl Phys 116:134104–134108

[26] Mallakpour S, Dinari M (2012) Fabrication of polyimide/titania nanocomposites containing benzimidazole side groups via sol–gel process. Prog Org Coat 75:373–378

[27] Yu JC, Ho W, Yu J, Yip H, Wong PK, Zhao J (2005) Efficient visible-light-induced photocatalytic disinfection on sulfur-doped nanocrystalline titania. Environ Sci Technol 39:1175–1179

[28] Li X, Wang N, Fan G, Yu J, Gao J, Sun G, Ding B (2015) Electreted polyetherimide-silica fibrous membranes for enhanced filtration of fine particles. J Colloid Interface Sci 439:12–20

[29] Vaquette C, Cooper-White JJ (2011) Increasing electrospun scaffold pore size with tailored collectors for improved cell penetration. Acta Biomater 7:2544–2557

[30] Mazoniene E, Bendoraitiene J, Peciulyte L, Diliunas S, Zemaitaitis A (2006) (Co)polyimides from commonly used monomers, and their nanocomposites. Prog Solid State Chem 34:201–211

[31] Ding M (2007) Isomeric polyimides. Prog Polym Sci 32:623–668

[32] Cha DI, Kim KW, Chu GH, Kim HY (2006) Mechanical behaviors and characterization of electrospun polysulfone/polyurethane blend nonwovens. Macromol Res 14:331–337

[33] Wan H, Wang N, Yang J, Si Y, Chen K, Ding B, Sun G, El-Newehy M, Al-Deyab SS, Yu J (2014) Hierarchically structured polysulfone/titania fibrous membranes with enhanced air filtration performance. J Colloid Interface Sci 417:18–26

[34] Pelaez M, Nolan NT, Pillai SC, Seery MK, Falaras P, Kontos AG, Dunlop PSM, Hamilton JWJ, Byrne JA, O'Shea K, Entezari MH, Dionysiou DD (2012) A review on the visible light active titanium dioxide photocatalysts for environmental applications. Appl Catal B 125:331–349

[35] Mohamed A, El-Sayed R, Osman TA, Toprak MS, Muhammed M, Uheida A (2016) Composite nanofibers for highly efficient photocatalytic degradation of organic dyes from contaminated water. Environ Res 145:18–25

[36] Ramirez AM, Demeestere K, De Belie N, Mäntylä T, Levänen E (2010) Titanium dioxide coated cementitious materials for air purifying purposes: preparation, characterization and toluene removal potential. Build Environ 45:832–838

[37] Nie L, Zheng Y, Yu J (2014) Efficient decomposition of formaldehyde at room temperature over Pt/honeycomb ceramics with ultra-low Pt content. Dalton Trans 43:12935–12942

[38] Dai Z, Huang C, Li M, Su J, Guo Y, Xu H, Ke Q (2016) Nanocrystalline MnO_2 on an activated carbon fiber for catalytic formaldehyde removal. RSC Adv. doi:10.1039/C6RA15463H